COLD SPRING HARBOR
Molecular Case Studies

RESEARCH ARTICLE

A patient with multisystem dysfunction carries a truncation mutation in human *SLC12A2*, the gene encoding the Na-K-2Cl cotransporter, NKCC1

Eric Delpire,[1] Lynne Wolfe,[2] Bianca Flores,[1] Rainelli Koumangoye,[1] Cara C. Schornak,[1] Salma Omer,[1] Barbara Pusey,[2] Christopher Lau,[2] Thomas Markello,[2] and David R. Adams[2]

[1]Department of Anesthesiology, Vanderbilt University School of Medicine, Nashville, Tennessee 37232, USA; [2]Undiagnosed Diseases Program, National Institutes of Health, Bethesda, Maryland 20892, USA

Abstract This study describes a 13-yr-old girl with orthostatic intolerance, respiratory weakness, multiple endocrine abnormalities, pancreatic insufficiency, and multiorgan failure involving the gut and bladder. Exome sequencing revealed a de novo, loss-of-function allele in *SLC12A2*, the gene encoding the Na-K-2Cl cotransporter-1. The 11-bp deletion in exon 22 results in frameshift (p.Val1026Phe*fs**2) and truncation of the carboxy-terminal tail of the cotransporter. Preliminary studies in heterologous expression systems demonstrate that the mutation leads to a nonfunctional transporter, which is expressed and trafficked to the plasma membrane alongside wild-type NKCC1. The truncated protein, visible at higher molecular sizes, indicates either enhanced dimerization or misfolded aggregate. No significant dominant-negative effect was observed. K^+ transport experiments performed in fibroblasts from the patient showed reduced total and NKCC1-mediated K^+ influx. The absence of a bumetanide effect on K^+ influx in patient fibroblasts only under hypertonic conditions suggests a deficit in NKCC1 regulation. We propose that disruption in NKCC1 function might affect sensory afferents and/or smooth muscle cells, as their functions depend on NKCC1 creating a Cl^- gradient across the plasma membrane. This Cl^- gradient allows the γ-aminobutyric acid (GABA) receptor or other Cl^- channels to depolarize the membrane affecting processes such as neurotransmission or cell contraction. Under this hypothesis, disrupted sensory and smooth muscle function in a diverse set of tissues could explain the patient's phenotype.

[Supplemental material is available for this article.]

Corresponding author: eric.delpire@vanderbilt.edu

Ontology terms: autonomic bladder dysfunction; chronic pain; orthostatic hypotension; small intestinal dysmotility

Published by Cold Spring Harbor Laboratory Press

doi: 10.1101/mcs.a001289

INTRODUCTION

SLC12A proteins are transmembrane proteins mediating the electroneutral transport of cations such as Na^+ and K^+, together with Cl^- in and out of cells (Lauf et al. 1992; Russell 2000). They play fundamental roles in a variety of physiological settings. SLC12A transporters participate in epithelial ion transport, modulate inhibitory synaptic transmission, and maintain and regulate cell volume (Haas and Forbush 2000; Markadieu and Delpire 2014; Kahle et al. 2015). Human mutations in two Na^+-independent K^+–Cl^- cotransporters KCC2 and KCC3 are involved in generalized idiopathic epilepsy (OMIM #616685) (Kahle et al. 2014), early infantile epileptic encephalopathy (OMIM #616645) (Stödberg et al. 2015), and

peripheral nerve degeneration (OMIM #218000) (Hubner et al. 2001; Woo et al. 2002; Boettger et al. 2003; Uyanik et al. 2006; Kahle et al. 2016), respectively. Mouse models of these disorders recapitulate the main aspects of the phenotypes (Hubner et al. 2001; Howard et al. 2002; Woo et al. 2002; Boettger et al. 2003; Kahle et al. 2016). Human mutations in two of the three Na^+-dependent cation Cl^- cotransporters are responsible for well-characterized salt-wasting disorders: Bartter syndrome (OMIM #607364) for NKCC2 (Simon et al. 1996a) and Gitelman syndrome (OMIM #263800) for NCC (Simon et al. 1996b), respectively. Mouse models accurately phenocopy these two disorders (Schultheis et al. 1998; Takahashi et al. 2000). One cation-chloride cotransporter that has eluded the list of cotransporters with human mutations is the ubiquitous Na-K-2Cl cotransporter-1 or NKCC1. NKCC1, like its family of transporters, plays a role in epithelial ion transport (O'Mahony et al. 2008; Bouyer et al. 2013; Kidokoro et al. 2014; Wei et al. 2015), modulates inhibitory synaptic transmission (Sung et al. 2000; Dzhala et al. 2005), and maintains and regulates cell volume (Wu et al. 1998; Bush et al. 2010; Mathieu et al. 2015). Accordingly, the knockout mouse exhibits multiple phenotypes that include sensorineural deafness (Delpire et al. 1999; Dixon et al. 1999; Flagella et al. 1999), male infertility (Pace et al. 2000), intestinal transit deficiency (Flagella et al. 1999; Wouters et al. 2006; Bradford et al. 2016), deficit in saliva secretion (Evans et al. 2000), and a pain perception phenotype (Sung et al. 2000; Laird et al. 2004; Granados-Soto et al. 2005). The absence of any report of human mutations in NKCC1 is puzzling and could indicate either complete intolerance to genetic variations (individuals selected out during gestation) or a large tolerance to genetic variations (many individuals carrying mutations without significant deleterious phenotypes). In this article, we report the case of a unique patient that carries a de novo truncation mutation in NKCC1.

RESULTS

Clinical Presentation and Family History

In 2010, an 8-yr-old female presented to the National Institutes of Health (NIH) Undiagnosed Diseases Program (UDP) with a complex syndrome including obstructive apnea, episodes of vomiting and dehydration, ketotic hypoglycemia with illness, decrease energy and fatigue, exercise intolerance, dilated cardiomyopathy (left ventricle dilation), and seizure-like episodes. Her prenatal/natal history was unremarkable: The maternal age was 35 yr (four pregnancies, four births), and the paternal age was 33 yr. Maternal weight gain was 25 lb, and fetal movements were described as normal. She was delivered after 38-wk gestation via Cesarean section (8 lb, 12 oz, 21 in, Apgar scores of 8 and 9) and discharged at 5 d following a mild jaundice. All developmental milestones were reached on time. Her symptoms began at ~6 mo of age. Extensive diagnostic and therapeutic medical interventions included a liver and muscle biopsy (Supplemental Table S5), and a gastric tube placed help manage and/or abort metabolic decompensations. Her dietary course was particularly challenging. Dietary intolerance prompted a progression from a high-protein formula to a free amino acid formula, and finally to total parenteral nutrition (TPN) at an age of 11 yr. Her weight is currently 40 kg (41st percentile). She is receiving 75 mL/kg/d of TPN with intermittent phosphate and essential fatty acid supplementation. Orthostatic intolerance is treated with intermittent 20 mL/kg i.v. fluid supplements. Heart rate and blood pressure lability are treated with daily midodrine, propranolol, and florinef (per jejunal tube). Respiratory support includes overnight bilevel positive airway pressure (BiPAP) for apnea and CO_2 retention. Cognitive function is normal. She attends school and shows normal locomotion and posture. Her vision, hearing, taste, and smell are seemingly normal, but she suffers from chronic pain treated with

scheduled i.v. fentanyl. Chronic nausea is treated with pantoprazole, granisetron, diphenhydramine, and ondansetron. Episodic anxiety is treated with diazepam.

Genomic Analysis

To identify potentially pathogenic DNA sequence variants coding mutations in the patient's genome, exome sequencing was performed on the patient, both unaffected parents, and three unaffected siblings. The genome fraction coverage data are provided in Supplemental Figure S1 and Supplemental Tables S1–S4. Variants that were rare, nonsynonymous, start-gain/loss, stop-gain/loss, frameshift, canonical splice site variants, or intronic variants (±20 bp) that were consistent with homozygous recessive, compound heterozygous, X-linked, or de novo dominant disease models were retained. Variant prioritization included factors such as population frequency, effect on amino acid coding, segregation, and predicted pathogenicity (Table 1). No clear pathogenic variants were found in known disease-causing genes. However, four mutations were prioritized for further analysis (Table 1, top four rows). The patient is compound heterozygous for variants in *PCNT* (pericentrin). PCNT is an integral component of the pericentriolar material that interacts with the microtubule nucleation component γ-tubulin. PCNT may be critical to the normal function of the centrosomes, cytoskeleton, and cell-cycle progression (Flory et al. 2000). Homozygous or compound heterozygous variants in PCNT have been reported in patients with microcephalic osteodysplastic primordial dwarfism type 2 (MOPD2, OMIM 210720) (Willems et al. 2010), making it unlikely that these heterozygous mutations account for the patient's disease. Two de novo mutations were also identified in the patient. First, we identified a missense mutation in *FMN2*, the gene encoding formin 2. FMN2 plays a role in cytoskeletal organization and the establishment of cell polarity (Law et al. 2014). Truncating variants in this gene were previously reported in patients with autosomal recessive mental retardation-47 (OMIM #616193) (Law et al. 2014), and there is no clear association to the clinical features of our patient. Second, a frameshift truncating variant in *SLC12A2*, the gene encoding the Na-K-2Cl cotransporter-1, was identified. As seen in Supplemental Figure S2, neither parents nor siblings carried the mutation, indicating that it originated de novo in germ cells. Among other processes, NKCC1 is involved in transcellular movement of chloride across both secretory and absorptive epithelia (Payne et al. 1995). The widespread expression and critical functionality of NKCC1, the deleterious nature, novelty, mode of inheritance, and high in silico deleteriousness score of the variant made the NKCC1 mutation the highest priority.

Functional Analysis of Mutant Transporter

To begin investigating the NKCC1 mutation, genomic DNA from the patient was used to polymerase chain reaction (PCR)-amplify and clone a fragment from the *SLC12A2* gene containing exon 22. Sequencing of randomly picked clones revealed both wild-type and mutant alleles, consistent with the heterozygous nature of her mutation. We thus confirmed that the patient carries an 11-bp deletion in exon 22, leading to the introduction of a premature stop codon and truncation of 200 amino acids of the cytosolic carboxyl terminus (Fig. 1A,B).

To assess the functionality of the mutant transporter (which we call NKCC1-DFX, as it terminates with an aspartic acid D followed by a phenylalanine F and a stop codon X), we injected groups of *Xenopus laevis* oocytes with NKCC1 (positive control) or NKCC1-DFX cRNAs. We then performed K^+-influx measurements under isotonic (200 mOsM) or hypertonic (270 mOsM) conditions in the presence or absence of 20 μM bumetanide. As seen in Figure 1C, we observed a sizable bumetanide-sensitive K^+ influx with wild-type cotransporter under isosmotic conditions that was significantly enhanced under hypertonic conditions. In contrast, we observed minimal bumetanide-sensitive K^+ influx with NKCC1-DFX under both

Table 1. Total list of variants

Gene	Chr Pos	HGVS cDNA	HGVS protein	CADD	ExAC All	ExAC European
SLC12A2	Chr5:127514355ATGTCTGGTGGC>A	NM_001046.2: c.3076_3086delGTCTGGTGGCT	p.V1026Ffs*2	36		
FMN2	Chr1:240371852C>T	NM_020066.4:c.3740C>T	p.P1247L	22.6		
PCNT	Chr21:47817316G>A	NM_006031.5:c.4354G>A	p.G1452R	23.8	384/121282 = 0.003	166/66660 = 0.002
PCNT	Chr21:47852019C>T	NM_006031.5:c.8641C>T	p.R2881W	25.2	1/120192 = 0	1/66000 = 0
RYR1	Chr19:39057626G>C	NM_000540.2:c.13513G>C	p.D4505H	23.4	281/46430 = 0.006	234/24010 = 0.01
RYR1	Chr19:39016132G>A	NM_000540.2:c.10616G>A	p.R3539H	26.1	209/116660 = 0.002	181/64324 = 0.003
ZC3H3	Chr8:144557667G>A	NM_015117.2:c.1804C>T	p.R602C	25.9	2/108464 = 0	1/60294 = 0
EGLN2	Chr19:41306234C>T	NM_053046.3:c.-234-10C>T		6.44		
EIF3J	Chr15:44829516C>T	NM_003758.3:c.44-6C>T		12.26		
HLA-DQA2	Chr6:32714664T>TTA	NM_020056.4:c.*326_*327insTA		1.061		
LOC100507547	Chr6:32121932C>T	NR_037169.1:c.197+14G>A		10.15		
RAB4B-EGLN2	Chr19:41306234C>T	NR_037791.1:c.815-10C>T		6.44		
RANBP2	Chr2:109384167C>G	NM_006267.4:c.7172C>G	p.T2391S	11.87	5/118310 = 0	3/64908 = 0
RANBP2	Chr2:109345582T>A	NM_006267.4:c.73-6T>A		12.74	453/106370 = 0.004	342/58144 = 0.006
ZBTB12	Chr6:31869122G>A	NM_181842.2:c.-20-20C>T		13.36	1349/99042 = 0.014	1087/55700 = 0.02

Total list of variants from the exome analysis that filters exome sequencing results by mode of inheritance, segregation with disease, population frequency (ExAC [Exome Aggregation Consortium], ESP6500, UDP [Undiagnosed Diseases Program] founders cohort), coding effects, and location (exonic, intronic, near splice). CADD (Combined Annotation-Dependent Depletion) (v1.3) scores the deleteriousness of single-nucleotide variants as well as insertion/deletions variants in the human genome.
HGVS, Human Genome Variation Society; cDNA, complementary DNA.

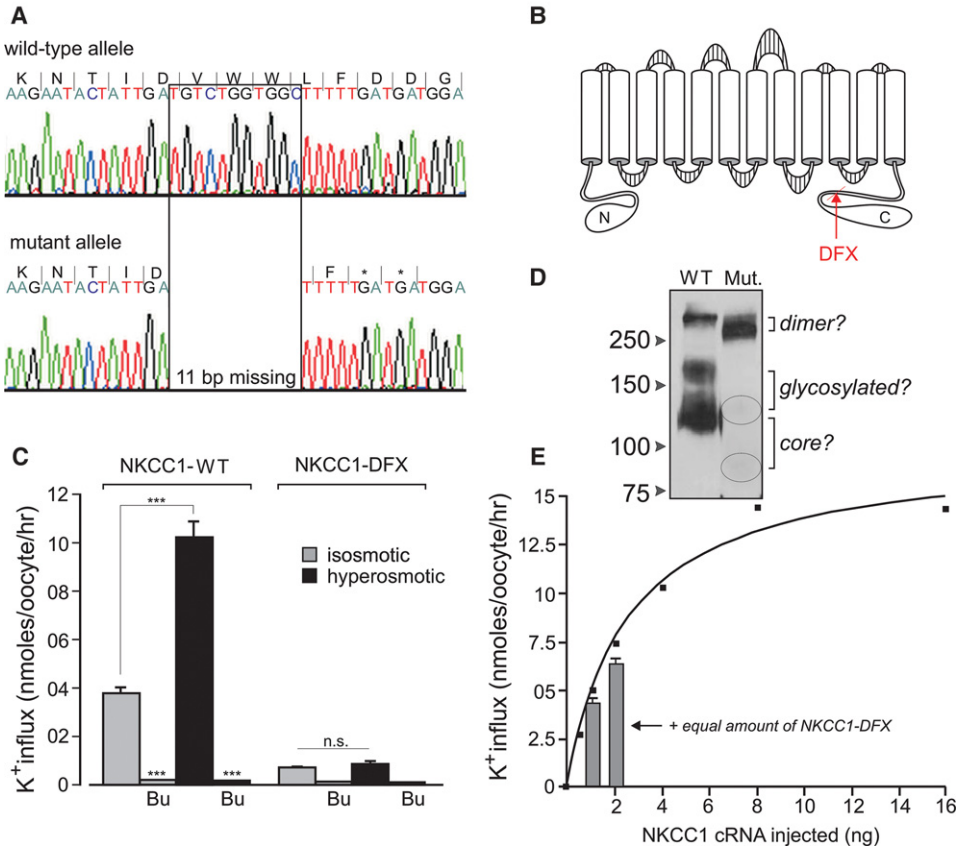

Figure 1. The NKCC1-DFX mutant is nonfunctional. (*A*) Sequence of a portion of *SLC12A2* exon 22 in patient shows wild-type allele (*top*) and 11-bp deletion in mutant allele (*bottom*). Translation results in a Phe residue inserted after Asp1025 followed by two stop codons (p.Val1026Phe*fs**2). (*B*) Schematic representation of the topology of human NKCC1 and position of the truncation. (*C*) Oocytes injected with wild-type but not mutant NKCC1 cRNA exhibit bumetanide-sensitive K^+ influx under isotonic and hypertonic conditions. Small bumetanide-sensitive component observed with mutant is due to native amphibian NKCC1. (*D*) Western blot analysis of oocyte lysates from wild-type and mutant NKCC1 complementary RNA (cRNA) injected oocytes. (*E*) Absence of significant dominant-negative effect of mutant NKCC1 on wild-type NKCC1 in *Xenopus laevis* oocytes. The curve represents a dose–response of K^+ influx versus amount of wild-type NKCC1 cRNA injected. The bars represent K^+ influx of oocytes injected with equivalent amount of mutant cotransporter cRNA. The bars represent means ± S.E.M. ($n = 20–25$ oocytes). (***) $P < 0.001$; n.s., nonsignificant; $P > 0.05$, one-way ANOVA followed by Tukey's multiple comparison posttests, WT, wild-type.

osmolarities. The very small bumetanide-sensitive component detected with NKCC1-DFX is due to native *Xenopus* NKCC1 (Gagnon et al. 2006).

The absence of cotransport function could be due to absence of expression of the mutant cotransporter. To address this possibility, we introduced a C-MYC epitope tag to the extreme amino-terminal tail of both wild-type and mutant cotransporters. As seen in Supplemental Figure S3, addition of the C-MYC tag did not alter the K^+ influx of wild-type NKCC1 under isotonic or hypertonic conditions. Western blot analysis of oocyte lysates expressing wild-type NKCC1 (Fig. 1D) revealed the presence of a major band between 100 and 150 kDa, representing the nonglycosylated form of the cotransporter, a second band slightly more than 150 kDa, corresponding to glycosylated transporter, and a third band of higher molecular size, corresponding to a cotransporter dimer (Kaplan et al. 1996a). In

contrast, lysates of oocytes injected with NKCC1-DFX cRNA revealed one major band corresponding to the dimer (or misfolded aggregate) and barely detectable glycosylated and core proteins. The three bands migrate at smaller molecular sizes, due to protein truncation (Fig. 1D).

As demonstrated in Figure 1A, the patient carries a normal allele from which full-length NKCC1 is expressed. To determine whether the mutant allele exerts any dominant-negative effect on wild-type cotransporter, we first injected oocytes with increasing amounts of wild-type NKCC1 cRNA. As seen in Figure 1E (curve), increasing amounts of cRNA resulted in increasing K^+ influx with signal saturation observed above 8 ng cRNA. We then coinjected 1 or 2 ng NKCC1-DFX alongside wild-type NKCC1 and observed similar levels of K^+ influx compared with wild-type NKCC1 alone, indicating no significant dominant-negative effect.

K^+ transport was next examined in fibroblasts from the patient using ^{86}Rb as a tracer in the presence or absence of transport inhibitors (Fig. 2A). The identity of the fibroblasts was verified using PCR and sequencing of exon 22 from genomic DNA isolated from the cells (Supplemental Fig. S4). Ouabain (an inhibitor of the Na^+/K^+-pump) and bumetanide (a NKCC-specific inhibitor) reduced K^+ transport in the patient fibroblasts by 50% and 41%, respectively. When combined, the drugs resulted in 86% reduction in K^+ influx, indicating that the wild-type allele of NKCC1 in the patient's fibroblasts is functional. When compared with control healthy human fibroblasts, obtained from the Vanderbilt UDP program, some significant differences were observed. First, the overall level of K^+ influx was reduced; second, the NKCC1-mediated influx was smaller than the pump-mediated influx; and third, under hypertonic conditions, no bumetanide-sensitive uptake could be detected (Fig. 2B). Note that no activation of K^+ influx was observed when exposing human fibroblasts to hypertonic conditions, a stimulus that typically leads to activation of NKCC1 (Gagnon and Delpire 2013). Altogether, our preliminary studies indicate that a functional NKCC1 is present, albeit to a lower level, in the patient's fibroblasts. The transporter behaves uncharacteristically under hypertonic conditions, as it loses its sensitivity to bumetanide.

To assess the presence of the mutant NKCC1-DFX at the plasma membrane, we cotransfected HeLa cells with tdTomato-NKCC1 and EGFP-NKCC1-DFX cDNA constructs and imaged the cells by confocal microscopy. As seen in Figure 2C, the two cotransporters colocalize at the plasma membrane of HeLa cells. This observation is significant because transporters with mutations in a conserved hydrophobic tetrad near the end of the carboxyl-terminal tail are unable to traffic properly to the plasma membrane (Nezu et al. 2009). Transporters without proper carboxy-terminal signals will not traffic from the endoplasmic reticulum to the golgi. The fact that both mutant and wild-type NKCC1 transporters are found at the cell surface in a cotransfection experiment suggests that a wild-type monomer with proper trafficking signals is able to carry a mutant monomer to the cell surface. These data, confirmed by a biotinylation experiment (Supplemental Fig. S5), are consistent with our observation that the mutant transporter facilitates (or stabilizes) the formation of dimers.

DISCUSSION

At this point, we cannot establish causality between the 11-bp deletion in exon 22 of *SLC12A2* and the clinical presentation of the patient, as this is based on one individual. Note that several frameshift and stop-gained mutations in human NKCC1 are listed in the Ensembl and Exome Aggregation Consortium (ExAC) databases (data summarized in Fig. 3). Although none of these mutations has been described in the literature, two of these individuals carrying premature stop codons (06-ST and 07-ST in Fig. 3) were from the 1000 Genomes Project (The 1000 Genomes Project Consortium 2010), which consisted of donors

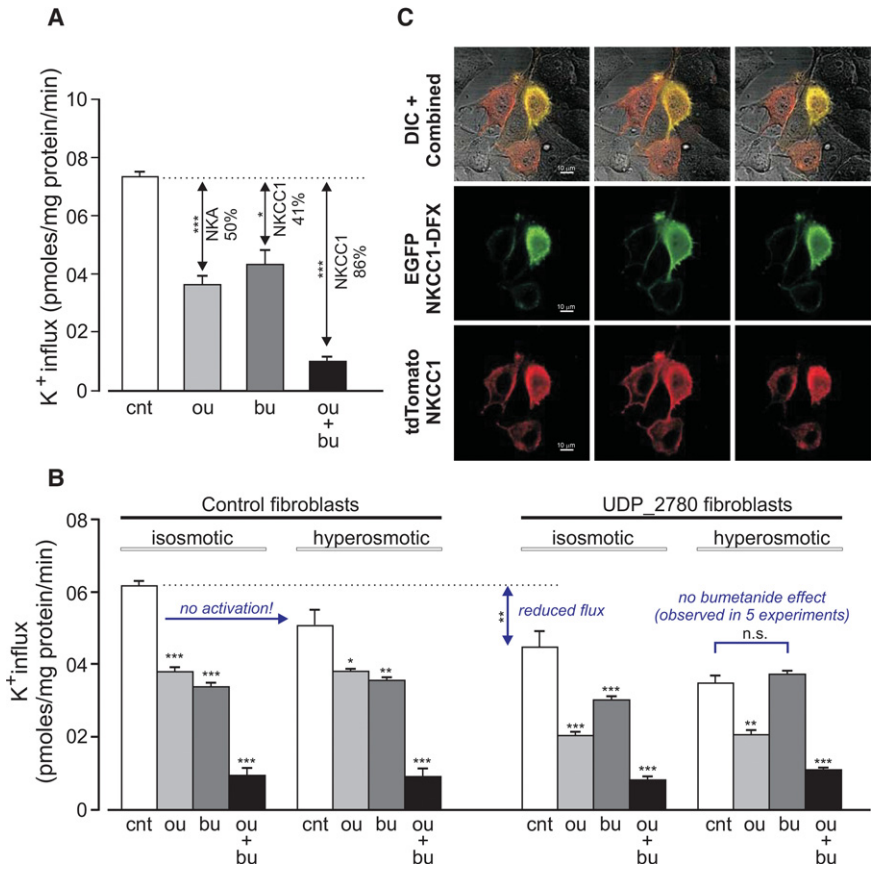

Figure 2. The behavior of the NKCC1-DFX mutant in human cells. (*A*) Characterization of major K^+ influx pathways in fibroblasts from patient. Flux was measured in control (cnt) conditions or the absence of inhibitors, in the presence of 1 mM ouabain (ou) to inhibit the Na^+/K^+ pump, in the presence of 20 µM bumetanide (bu) to inhibit NKCC1, and in the presence of both inhibitors (ou + bu). (***) $P < 0.001$; (*) $P < 0.05$, one-way ANOVA followed by Tukey's multiple comparison posttests. (*B*) Similar experiment performed under isosmotic (310 mOsM) and hyperosmotic (385 mOsM) conditions in fibroblasts from UDP_2780 patient compared with control human fibroblasts. Bars represent means ± S.E.M ($n = 3$ dishes). (***) $P < 0.001$, (**) $P < 0.01$, (*) $P < 0.05$, n.s., nonsignificant; $P > 0.05$, one-way ANOVA followed by Tukey's multiple comparison posttests. (*C*) Fluorescence images of HeLa cells transfected with tdTomato-NKCC1 (red) and EGFP-NKCC1-DFX (green). Images captured at three consecutive *Z*-sections with confocal microscopy reveals colocalization at the plasma membrane. Scale bar, 10 µm.

that were more than 18 years of age and classified as healthy at the time of DNA collection. This observation indicates that inactivation of one allele alone is unlikely sufficient to account for the patient's condition. This agrees with knockout *Slc12a2* (NKCC1) mice, which exhibit little to no overt phenotype as heterozygotes but demonstrate strong phenotypes as homozygotes (Delpire et al. 1999; Dixon et al. 1999; Flagella et al. 1999). The patient does not suffer from the inner ear deficit that characterizes the homozygous NKCC1 knockout mouse (Delpire et al. 1999; Dixon et al. 1999; Flagella et al. 1999), but she demonstrates the low blood pressure and gastrointestinal function deficits reminiscent of the null mice (Flagella et al. 1999; Wouters et al. 2006; Garg et al. 2007). In fact, the common gastrointestinal deficit is interesting in light of a recent report showing up-regulation of digestive enzymes produced by the exocrine pancreas of the NKCC1 knockout mouse, possibly as a way to compensate for reduced intestinal function (Bradford et al. 2016).

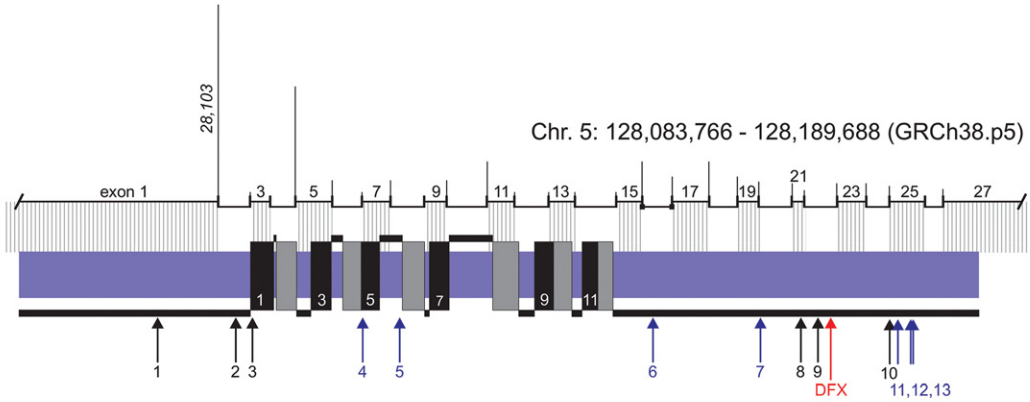

Database	Exon	Variation	Alleles	Codons	AA mutation	Origin	Allele Count
01-FS	1 exon 1	DELETION	GACAC/-	GACACg/g	Asp176Gly*fs*24		
02-FS	1-2 exon 2	rs750685012	-/GT	acg/acGTg	Tyr275Cys*fs*11	European	1 / 121,288
03-FS	1 exon 2	rs762969008	-/G	aag/aaGg	Val291Cys*fs*16		
04-ST	1-2 exon 7	rs752246285	C/T	Cag/Tag	Gln435X	European	1 / 121,132
05-ST	1-2 exon 8	rs747216802	C/T	Cga/Tga	Arg482X	European	2 / 121,228
06-ST	1 exon 16	rs545485266	T/G	tTa/tGa	Leu804X	Finland	
07-ST	1-2 exon 20	rs560689091	T/A	tTa/tAa	Leu937X	Bengali	
08-FS	1-2 exon 21	rs755730597	-/GA	cca/cGAca	Pro988Arg*fs*5	Latino	1 / 121,116
09-FS	1-2 exon 22	rs778899336	A/-	cAa/ca	Lys1007Ser*fs*30	European	1 / 120,296
10-FS	1-2 exon 24	rs776861731	AAAG/-	ccAAAG/cc	Glu1099Ile*fs*4	African	1 / 108008
11-ST	1-2 exon 25	rs749878530	-/A	tac/tAac	Tyr1111X	European	1 / 119,898
12-ST	1-2 exon 25	rs760131732	-/36 bp		Asp1129Tyr*fs*2		
13-ST	1-2 exon 25	rs747023237	C/T	Cga/Tga	Arg1133X	African	1 / 119,614

Figure 3. Additional SLC12A2 frameshift and stop codon variants in human population. The Ensembl genome browser database (species/gene/transcript/exons) color lists a large number of variants for each human gene, and we identified 13 unique variations leading to NKCC1 truncation. The majority of these mutations are also reported in the ExAC database (http://exac.broadinstitute.org/). These variants are labeled 1–13, and their position in the protein is indicated by arrows. The location of the NKCC1-DFX mutation is shown by the red arrow. The 12 transmembrane domains are designated by alternate black and gray boxes crossing the plasma membrane (blue). The location of the exons is indicated above the protein with size of introns proportionally drawn as vertical lines. DNA and amino acid sequence of the 13 variants are listed under the (1) Ensembl database and/or (2) ExAC database.

Because of metabolic issues, the patient underwent muscle and liver biopsies to investigate possible mitochondrial dysfunction. Most of her tests fell within normal range, except for increased mitochondrial DNA copy number, elevated muscle glycogen content, and increased levels of coenzyme Q10. Increased mtDNA copy number could indicate a feedback mechanism to compensate for defects in mitochondrial respiratory function. However, all enzymes measured associated with the complexes of the respiratory chain were normal. The exception was for coQ10 levels, which were significantly increased. CoQ10 is a cofactor that passes electrons between mitochondrial complexes and thus constitutes a key component of mitochondrial respiration. Increased coQ10 levels could reflect an overall increase in the number of mitochondria or an attempt to increase efficiency of the respiratory chain. In light of the otherwise normal levels of all other enzymes, it is unclear whether mitochondrial respiration and production of ATP is affected in the patient. Reduced mitochondrial respiration could explain why glycogen (energy storage) is increased in both liver and muscle. To date there is no known link between NKCC1-mediated transport and mitochondrial function. However, one could conceive that disturbed intracellular Na^+ levels could affect intramitochondrial Ca^{2+} levels and in turn affect the respiratory chain.

The fact that no humans with complete loss of function of NKCC1 (NKCC1 knockouts) have been identified suggests intolerance to functional variation, at least in the homozygous

state. If the NKCC1 mutation truly contributes to the patient's condition, why would some individuals with one deficient allele be affected and others would not? It is possible that additional environmental or genetic conditions that are particular to the patient have contributed to the development of the disease. Alternatively, it is also possible that this specific NKCC1 mutant protein could be expressed, whereas other mutations in the gene result in unstable transcripts or proteins. Expression of the mutant protein would then lead to deleterious effects on ion transport or cell metabolism. We found that the mutant protein is translated, at least in heterologous expression systems, and is trafficked alongside the wild-type cotransporter to the plasma membrane (seen in Fig. 2C). In addition, we found a greater amount of protein expression, possibly indicative of a dimer, in both mutant NKCC1-injected oocytes (Fig. 1D) and patient fibroblasts (Supplemental Fig. S4). Because the functional unit of NKCC1 is a homodimer (Moore-Hoon and Turner 2000), and the carboxy-terminal tail is involved in the formation of dimers (Simard et al. 2004), we propose that the mutant transporter is trafficked to the plasma membrane only when complexed with a wild-type monomer, thereby affecting the regulation of the transporter at the cell surface. Because the K^+ transport did not respond to bumetanide under hypertonic conditions in the patient's fibroblasts, this indicates transport dysregulation. The bumetanide-insensitivity of mutant NKCC1 under hypertonicity is puzzling and should be pursued as it is likely to provide useful information about the biology of the cotransporter. This observation was unexpected because bumetanide is thought to interact with the cotransporter within an extracellular gate that includes residues lining transmembrane domain 3 (Somasekharan et al. 2012). Thus, our data would suggest that large changes in the cytosolic carboxy-terminal portion of the cotransporter might affect the conformation of the membrane portion of the cotransporter enough to possibly occlude the bumetanide binding site. Although the hypertonic treatment is nonphysiological, it is a test that is commonly used to assess the ability of the transporter to be activated by a series of regulatory kinases that modulate NKCC1 function. Thus, the function of NKCC1 might be more affected in some cells than others. Although we did not see a very significant reduction in cotransporter function in the patient's fibroblasts, only subtle deficits in regulation, cotransporter function may be affected in other cell types. Note that the truncation in NKCC1-DFX occurs downstream of a signal sequence within exon 21 that targets the transporter to the basolateral membrane of epithelial cells (Carmosino et al. 2008). This sequence is absent in NKCC2, a cotransporter expressed on the apical membrane of the thick ascending limb of Henle in kidney (Kaplan et al. 1996b; Carmosino et al. 2008). Some tissues (e.g., brain) express an isoform of *NKCC1* lacking exon 21 (Randall et al. 1997) with one possible candidate tissue being choroid plexus as it abundantly expresses NKCC1 on the apical membrane (Plotkin et al. 1997). Whether the mutant transporter is expressed and mistargeted in epithelial cells in the patient will need to be examined. The timeline of organ failure, which has accelerated in the past few years, is consistent with existing function of the cotransporter and suggests that factors such as stress on tissues or organs might be involved in the progression of the disease.

We present two major hypotheses to account for the multisystem failure in the patient. First, each tissue/organ that has failed in the patient sends sensory afferent fibers to the spinal cord. These sensory neurons have their cell bodies located in the dorsal root ganglia associated with the specific vertebrae segment(s) innervating these organs. It is known from the pioneer work of Javier Alvarez-Leefmans in amphibians that dorsal root ganglion neurons accumulate intracellular Cl^- in a Na^+-, K^+-, and furosemide-dependent manner (Alvarez-Leefmans et al. 1988). By using a NKCC1-specific antibody, we confirmed that the transporter involved in this accumulation is NKCC1 (Plotkin et al. 1997). We also demonstrated abnormal γ-aminobutyric acid (GABA) responses associated with a collapsed Cl^- gradient in DRG neurons isolated from NKCC1 knockout mice (Sung et al. 2000). While the role of NKCC1 in DRG neurons has been almost exclusively examined in relation to the transfer of pain signals

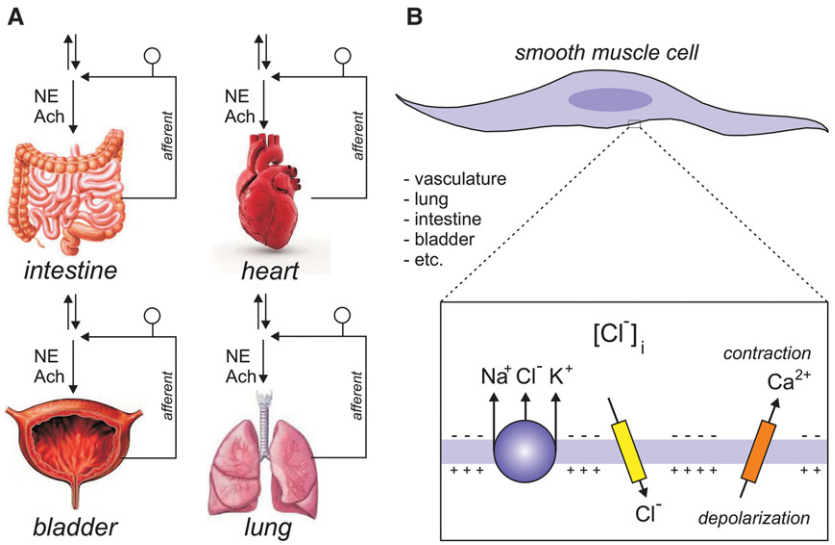

Figure 4. Two models are described to account for how NKCC1 function leads to multiorgan failure. (*A*) Each organ sends afferent fibers to the spinal cord to modulate autonomic function. These neurons have their cell bodies in dorsal root ganglia. Parallel arrows indicate spinal cord ascending and descending pathways. (*B*) All major organs have smooth muscle cells where NKCC1 accumulates Cl^- above thermodynamic potential equilibrium. Opening of Cl^- channels depolarizes the membrane triggering the opening of voltage-sensitive Ca^{2+} channels, Ca^{2+} entry, and contraction. NKCC1 dysfunction leads to collapse of Cl^- gradients in both sensory (DRG) neurons and smooth muscle cells, thereby contributing to the multiorgan pathology.

from afferent fibers to the spinal cord (Alvarez-Leefmans 2009; Delpire and Austin 2010), it is likely that NKCC1 fulfills a similar role in sensory innervation of tissues like the heart, lung, bladder, and intestine (Fig. 4A). Note that, consistent with a role for NKCC1 in filtering the transfer of pain signals from the periphery to the central nervous system, we report that the patient suffers from chronic pain. Our second hypothesis, which is by no means exclusive of the first, involves smooth muscle cell contraction (Fig. 4B). In these cells, NKCC1 also accumulates intracellular Cl^- above thermodynamic potential equilibrium, thereby facilitating Cl^- channel depolarization and triggering of Ca^{2+} channels, leading to Ca^{2+} entry and smooth muscle cell contraction (Akar et al. 2001; Ferrera et al. 2010; Bulley and Jaggar 2014). Thus, weakening of NKCC1 function in smooth muscle cells will likely affect their ability to contract affecting multiple tissues that rely on smooth muscle cell function, such as vasculature, lung, intestine, and bladder. Each of these hypotheses in relationship to the patient mutation will be addressed in future work.

METHODS

Exome Sequencing and Analysis

The Undiagnosed Disease Program assigned the number UDP_2780 to this patient. Whole blood was collected from patients and family members, and then DNA extraction was carried out using the Autogen FlexStar automated system following Autogen's standard DNA extraction method. The DNA samples were then subjected to phenol–chloroform purification and sent to the NIH Intramural Sequencing Center (NISC) for massively paralleled sequencing. Exome libraries with ~300-bp inserts and paired-end index adapters were prepared according to Illumina's TruSeq DNA Sample Preparation v1 or v2 method and sequenced on a

HiSeq2000 sequencer (Illumina) for 101-bp paired-end reads. The sequencing reads then were filtered for quality, and aligned to human reference genome NCBI build 37 (hg19) using in-house developed pipelines, one based on Novoalign (Novocraft Technologies), and separately a diploid aligner (Pemberton et al. 2014) run on a commercial platform (Appistry Inc.). Variants were called with HaplotypeCaller and GenotypeGVCFs (McKenna et al. 2010; DePristo et al. 2011; Van der Auwera et al. 2013). Annotations utilized SnpEff (Cingolani et al. 2012) and a combination of publicly available data sources (EXaC, ESP, 1000 Genomes). Internal cohort statistics were utilized for variant filtration. Taken together, rare, nonsynonymous, start-gain/loss, stop-gain/loss, frameshift, canonical splice site variants, and intronic variants (±20 bp) that were consistent with homozygous recessive, compound heterozygous, X-linked, or de novo dominant disease models were retained. The variants were then manually inspected using the Integrative Genomics Viewer (IGV) and checked for publicly available clinical or functional data in OMIM (Online Mendelian Inheritance in Man), HGMD (Human Gene Mutation Database), and PubMed.

SLC12A2 Confirmation Sequencing Primers

The following primers were used by the UDP program to verify the *SLC12A2* mutation—forward: 5′ GGAATTCAGCAAAAGGGACT 3′; and reverse: 5′ AACCTTACCTCCATCATC AAAAA 3′. A different primer set was used at Vanderbilt to verify the mutation in the proband's DNA and fibroblast samples: forward 5′ AACATTAGGAAATGATAGGAATTCAGC 3′; and reverse: 5′ TCATTTCTTACTATTCTCACAATGTCAG 3′.

NKCC Function in Fibroblasts

Fibroblasts from UDP_2780 patient and from controls were cultured in 10-cm dishes in DMEM:F12 medium containing 10% fetal bovine serum and 200 U penicillin + 200 µg/mL streptomycin and kept at 37°C under 95% air, 5% CO_2. NKCC1 function was determined using bumetanide-sensitive K^+ influx. Smaller dishes (35-mm) were coated with 1 mL poly-L-Lysine (0.1 mg/mL) overnight in the 37°C incubator. The next day, the dishes were washed twice with 1 mL sterile water and 2 mL of a high-density suspension of fibroblasts (1 × 10-cm confluent dish resuspended in 16 mL to plate 8 × 35-mm dishes) was plated in each dish. Three dishes were plated per experimental condition. Thus, all dishes were plated with equal amount of cells, minimizing variability between dishes. The cells were allowed to attach for 2 h in complete culture medium, at 37°C under 95% air, 5% CO_2. For the flux, culture medium was aspirated from triplicate dishes and replaced with 1 mL isosmotic saline (140 mM NaCl, 5 mM KCl, 2 mM $CaCl_2$, 1 mM $MgCl_2$, 2 mM glucose, 5 mM HEPES—pH 7.4, 310 mOsM) or hypertonic saline (isotonic + 75 mM sucrose, 385 mOsM) for a 15 min preincubation. The preincubation solution was aspirated prior to the addition of an identical saline containing 1 mCi/mL ^{86}Rb in the absence or presence of 1 mM ouabain and 20 µM bumetanide. After 15 min uptake, the solution was aspirated and the dishes washed three times with ice-cold saline. Conditions were staggered every 2 min, allowing manipulation of solutions. Dishes were kept dry until all dishes had been fluxed. At the end of the ^{86}Rb uptake, 500 µL NaOH was added per dish for 1 h at RT under gentle shaking, followed by addition of 250 µL acetic acid (glacial). Samples of 300 µL and 30 µL were used for β-scintillation counting and protein assay (Bio-Rad), respectively. Influx was expressed in picomoles K^+ per milligram protein per minute.

Fluorescence Microscopy

HeLa cells plated onto glass-bottom microwell 35-mm dishes (MatTek) were transfected with 2 µg each cDNA encoding tdTomato-fused wild-type NKCC1, EGFP-fused mutant NKCC1-DFX, and 12 µL FuGene 6.0 (ratio DNA:Fugene = 1:3; Roche Applied Science). Two days

posttransfection, the cells were imaged on a Zeiss LSM 710 confocal microscope. Images were captured using a 63× oil objective (numerical aperture, 1.4) in the green fluorescent protein (GFP) (488 nm) or tdTomato (565 nm) channel using a Zeiss laser scanning LSM 710 META inverted confocal microscope.

Creation of the Mouse Mutant NKCC1 cDNA

We started from the cDNA encoding full-length wild-type mouse NKCC1 inserted into pBF (Delpire et al. 1994), a vector that contains 5′- and 3′-untranslated regions from the *Xenopus* β-globin gene. Overall, mouse NKCC1 is highly conserved at the protein level (94% identity–96% homology with human NKCC1). We took advantage of a unique NheI site located 40-bp upstream of the 11-bp deletion and a unique XhoI site located after the stop codon to eliminate a 606-bp coding fragment (202 amino acids). The coding fragment was replaced with an adaptor made of two complementary oligonucleotides: forward 5′ CTAGCACACAG TTTCAGAAAAAACAAGGGAAGAATACTATAGATTTTTGAC 3′ and reverse 5′ TCGAGT CAAAAATCTATAGTATTCTTCCCTTGTTTTTTCTGAAACTGTGTG 3′. The adapter restores some 15 amino acids and adds a novel phenylalanine residue before a stop codon to mimic the patient's mutation. The mutant clone was sequenced to verify proper insertion of the adapter. To create c-myc-tagged constructs, we started from an EGFP-NKCC1 fusion construct (Gagnon et al. 2006) and replaced the open reading frame of EGFP by using EcoRI and BglII and ligating an adaptor made of two complementary oligonucleotides encoding the C-MYC epitope: EQKLISEEDL. The DFX mutation was then added as described above.

Xenopus laevis Oocytes

Oocyte-positive *Xenopus laevis* female frogs were maintained in static aquaria as previously described (Delpire et al. 2011). For surgery, frogs were anesthetized with buffered tricaine (1.7 g/L + 3.4 g/L Na-bicarbonate), placed on a wet stack of paper placed on ice, and a small 4- to 6-mm incision was made on the lower abdomen by using a disposable sterile scalpel (Feather #11; Fisher Scientific). Ovarian lobes were externalized with sterile curved forceps, removed with sharp scissors, and placed in a 10-cm plastic culture dish containing divalent-free ND96 (96 mM NaCl, 4 mM KCl, HEPES 5 mM, pH 7.4—185 mOsM).The incision was sutured with three to four stitches by using 4–0 monofilament nylon surgical suture (DemeTech; 18-mm needle, three-eighth circle, reverse cutting). After the frogs recovered from anesthesia in shallow water, they were returned to their housing and recovered for a minimum of 8 wk. Oocytes (stages V–VI; $n = 20–25$) were defolliculated by 4 × 90-min treatments (vigorous shaking at 4°C) with 5 mL divalent-free ND96 containing 9.5 mg/mL collagenase D with washes between treatments. After the final wash, oocytes were placed in modified L15 (250 mL Leibovitz L15 Ringer [Invitrogen], 200 mL deionized water, 952 mg HEPES [acid form], and 400 µL of 50 mg/mL gentamycin [Invitrogen]; pH 7.0; 195–200 mOsM), filtered on 0.22 µm cellulose acetate membrane and allowed to recover overnight in a 16°C incubator.

cRNA Transcription and Injection

cDNA clones inserted in pBF were linearized with the restriction enzyme MluI and linearized DNA (2.5 µg) was transcribed into cRNA using the mMessage mMachine SP6 transcription kit (Ambion). cRNA quality was verified by gel electrophoresis (1% agarose, 0.693% formaldehyde) and quantitated by measurement of absorbance at 260, 280, and 320 nm. The day after isolation, oocytes were injected with 50 nL water or cRNA mixture (15 ng cRNA or as indicated) by using a 10-µL digital microdispenser (Drummond Scientific) fitted with sterile pulled glass capillary tubes.

Western Blot Analysis

Groups of 10 oocytes injected with C-MYC-NKCC1 or C-MYC-NKCC1-DFX were placed in the bottom of an Eppendorff tube and excess saline was removed. Lysis solution (200 µL or 20 µL per oocyte) was added to the tube and oocytes were broken by vigorous pipetting through a 200-µL pipet tip. The lysis solution contained 100 mM NaCl, 50 mM TrisCl pH 7.6, 20 mM EDTA, 1% Triton X-100, 0.1 sodium dodecyl sulfate (SDS), and protease inhibitor (Roche). After 30 min incubation on ice, the tubes were centrifuged at 14,000 rpm for 20 min at 4°C and the supernatant was passed through a minicolumn to capture oocyte lipids. Equal volume (20 µL) lysate was subjected to 6% SDS-polyacrylamide gel electrophoresis (PAGE) and the gel was transferred to a polyvinylidene fluoride (PVDF) membrane (ThermoFisher Scientific). The membrane was probed with mouse monoclonal anti-C-MYC (clone 9E10; ThermoFisher Scientific), followed by horseradish peroxidase (HRP)-conjugated secondary anti-mouse antibody (Jackson ImmunoResearch), and revealed using enhanced chemiluminescence (PerkinElmer).

K^+ Influx Measurements in Oocytes

Unidirectional ^{86}Rb uptake was measured in groups of 20 to 25 oocytes. Oocytes placed in a 35-mm dish were washed once with 3 mL isosmotic saline (96 mM NaCl, 4 mM KCl, 2 mM $CaCl_2$, 1 mM $MgCl_2$, 5 mM HEPES; pH 7.4) and preincubated for 15 min in 1 mL isosmotic saline containing 1 mM ouabain (to inhibit K^+ uptake through the Na^+/K^+ pump). The solution was then aspirated and replaced with 1 mL isosmotic or hypertonic (+70 mM sucrose) flux solution containing 5 µCi ^{86}Rb. Two 5-µL aliquots of uptake solution were taken at the beginning of each ^{86}Rb-uptake to be used as standards. After 1 h, the radioactive solution was aspirated, and the oocytes were washed four times with 3 mL ice-cold solution. Oocytes were transferred into individual glass vials, lysed for 1 h with 200 µL 0.25 N NaOH, and neutralized with 100 µL glacial acetic acid. ^{86}Rb tracer activity was measured by β-scintillation. K^+ influx was calculated from counts in oocytes and standards and expressed in nanomoles per oocyte per hour.

Statistical Analyses

One-way ANOVA (GraphPad Prism version 7.0, GraphPad Software, Inc) followed by Tukey's multiple comparisons test was used to assess statistical significance among groups in K^+ flux data. We considered $P < 0.05$ to be statistically significant.

ADDITIONAL INFORMATION

Data Deposition and Access

The patient genomic variants were deposited in the Database of Genotypes and Phenotypes (dbGaP) (http://www.ncbi.nlm.nih.gov/gap) under accession number phs000721.v1.p1, in ClinVar (https://www.ncbi.nlm.nih.gov/clinvar/) under accession number SCV000328200, and in the PhenomeCentral database (https://www.phenomecentral.org/) under accession number P0003119.

Ethics Statement

The patient provided written consent for tissue sampling and genomic analysis. Institutional Review Board approval was obtained at the National Institutes of Health for Protocol 76–HG–0238: "Diagnosis and Treatment of Patients with Inborn Errors of Metabolism or Other Genetic Disorders."

Competing Interest Statement

The authors have declared no competing interest.

Referees

Ralph J. DeBerardinis
Anonymous

Received July 26, 2016; accepted in revised form October 10, 2016.

Acknowledgments

Fluorescence imaging was performed using the Vanderbilt Cell Imaging Shared Resource.

Author Contributions

All authors contributed data, were involved in writing, and approved the submitted versions of this article.

Funding

This work was supported by National Institutes of Health (NIH) grants RO1DK093501 and R21GM118944 to E.D. B.F. is supported by NIH grant T32MH064913.

REFERENCES

Akar F, Jiang G, Paul RJ, O'Neill WC. 2001. Contractile regulation of the Na^+-K^+-$2Cl^-$ cotransporter in vascular smooth muscle. *Am J Physiol Cell Physiol* **281:** C579–C584.

Alvarez-Leefmans FJ. 2009. Chloride transporters in presynaptic inhibition, pain and neurogenic inflammation. In *Physiology and pathology of chloride transporter and channels in the nervous system: from molecules to diseases* (ed. Alvarez-Leefmans FJ, Delpire E, Alvarez-Leefmans FJ, Delpire E), pp. 439–470. Academic, London.

Alvarez-Leefmans FJ, Gamiño SM, Giraldez F, Nogueron I. 1988. Intracellular chloride regulation in amphibian dorsal root ganglion neurons studied with ion-selective microelectrodes. *J Physiol (Lond)* **406:** 225–246.

Boettger T, Rust MB, Maier H, Seidenbecher T, Schweizer M, Keating DJ, Faulhaber J, Ehmke H, Pfeffer C, Scheel O, et al. 2003. Loss of K-Cl co-transporter KCC3 causes deafness, neurodegeneration and reduced seizure threshold. *EMBO J* **22:** 5422–5434.

Bouyer PG, Tang X, Weber CR, Shen L, Turner JR, Matthews JB. 2013. Capsaicin induces NKCC1 internalization and inhibits chloride secretion in colonic epithelial cells independently of TRPV1. *Am J Physiol Gastrointest Liver Physiol* **304:** G142–G156.

Bradford EM, Vairamani K, Shull GE. 2016. Differential expression of pancreatic protein and chemosensing receptor mRNAs in NKCC1-null intestine. *World J Gastrointest Pathophysiol* **7:** 138–149.

Bulley S, Jaggar JH. 2014. Cl^- channels in smooth muscle cells. *Pflügers Arch Eur J Physiol* **466:** 5861–5872.

Bush PG, Pritchard M, Loqman MY, Damron TA, Hall AC. 2010. A key role for membrane transporter NKCC1 in mediating chondrocyte volume increase in the mammalian growth plate. *J Bone Miner Res* **25:** 1594–1603.

Carmosino M, Giménez I, Caplan M, Forbush B. 2008. Exon loss accounts for differential sorting of Na-K-Cl cotransporters in polarized epithelial cells. *Mol Biol Cell* **19:** 4341–4351.

Cingolani P, Platts A, Wang le L, Coon M, Nguyen T, Wang L, Land SJ, Lu X, Ruden DM. 2012. A program for annotating and predicting the effects of single nucleotide polymorphisms, SnpEff: SNPs in the genome of *Drosophila melanogaster* strain w1118; iso-2; iso-3. *Fly (Austin)* **6:** 80–92.

Delpire E, Austin TM. 2010. Kinase regulation of Na^+-K^+-$2Cl^-$ cotransport in primary afferent neurons. *J Physiol* **588:** 3365–3373.

Delpire E, Rauchman MI, Beier DR, Hebert SC, Gullans SR. 1994. Molecular cloning and chromosome localization of a putative basolateral Na-K-2Cl cotransporter from mouse inner medullary collecting duct (mIMCD-3) cells. *J Biol Chem* **269:** 25677–25683.

Delpire E, Lu J, England R, Dull C, Thorne T. 1999. Deafness and imbalance associated with inactivation of the secretory Na-K-2Cl co-transporter. *Nat Genet* **22:** 192–195.

Delpire E, Gagnon KB, Ledford J, Wallace J. 2011. Housing and husbandry of *Xenopus laevis* impact the quality of oocytes for heterologous expression studies. *J Am Assoc Lab Anim Sci* **50:** 46–53.

DePristo MA, Banks E, Poplin R, Garimella KV, Maguire JR, Hartl C, Philippakis AA, del Angel G, Rivas MA, Hanna M, et al. 2011. A framework for variation discovery and genotyping using next-generation DNA sequencing data. *Nat Genet* **43:** 491–498.

Dixon MJ, Gazzard J, Chaudhry SS, Sampson N, Schulte BA, Steel KP. 1999. Mutation of the Na-K-Cl co-transporter gene Slc12a2 results in deafness in mice. *Hum Mol Genet* **8:** 1579–1584.

Dzhala VI, Talos DM, Sdrulla DA, Brumback AC, Mathews GC, Benke TA, Delpire E, Jensen FE, Staley KJ. 2005. NKCC1 transporter facilitates seizures in the developing brain. *Nat Med* **11:** 1205–1213.

Evans RL, Park K, Turner RJ, Watson GE, Nguyen H-V, Dennett MR, Hand AR, Flagella M, Shull GE, Melvin JE. 2000. Severe impairment of salivation in $Na^+/K^+/2Cl^-$ cotransporter (NKCC1)-deficient mice. *J Biol Chem* **275:** 26720–26726.

Ferrera L, Caputo A, Galietta LJ. 2010. TMEM16A protein: a new identity for Ca^{2+}-dependent Cl^- channels. *Physiology (Bethesda)* **25:** 357–363.

Flagella M, Clarke LL, Miller ML, Erway LC, Giannella RA, Andringa A, Gawenis LR, Kramer J, Duffy JJ, Doetschman T, et al. 1999. Mice lacking the basolateral Na-K-2Cl cotransporter have impaired epithelial chloride secretion and are profoundly deaf. *J Biol Chem* **274:** 26946–26955.

Flory MR, Moser MJ, Monnat RJ Jr, Davis TN. 2000. Identification of a human centrosomal calmodulin-binding protein that shares homology with pericentrin. *Proc Natl Acad Sci* **97:** 5919–5923.

Gagnon KB, Delpire E. 2013. Physiology of SLC12 transporters: Lessons from inherited human genetic mutations and genetically-engineered mouse knockouts. *Am J Physiol Cell Physiol* **304:** C693–C714.

Gagnon KB, England R, Delpire E. 2006. Volume sensitivity of cation-chloride cotransporters is modulated by the interaction of two kinases: SPAK and WNK4. *Am J Physiol Cell Physiol* **290:** C134–C142.

Garg P, Martin CF, Elms SC, Gordon FJ, Wall SM, Garland CJ, Sutliff RL, O'Neill WC. 2007. Effect of the Na-K-2Cl cotransporter NKCC1 on systemic blood pressure and smooth muscle tone. *Am J Physiol Heart Circ Physiol* **292:** H2100–H2105.

Granados-Soto V, Arguelles CF, Alvarez-Leefmans FJ. 2005. Peripheral and central antinociceptive action of Na-K-2Cl cotransporter blockers on formalin-induced nociception in rats. *Pain* **114:** 231–238.

Haas M, Forbush BI. 2000. The Na-K-Cl cotransporter of secretory epithelia. *Annu Rev Physiol* **62:** 515–534.

Howard HC, Mount DB, Rochefort D, Byun N, Dupré N, Lu J, Fan X, Song L, Rivière J-B, Prévost C, et al. 2002. Mutations in the K-Cl cotransporter KCC3 cause a severe peripheral neuropathy associated with agenesis of the corpus callosum. *Nat Genet* **32:** 384–392.

Hubner CA, Stein V, Hermans-Borgmeyer I, Meyer T, Ballanyi K, Jentsch TJ. 2001. Disruption of KCC2 reveals an essential role of K-Cl cotransport already in early synaptic inhibition. *Neuron* **30:** 515–524.

Kahle KT, Merner ND, Friedel P, Silayeva L, Liang B, Khanna A, Shang Y, Lachance-Touchette P, Bourassa C, Levert A, et al. 2014. Genetically encoded impairment of neuronal KCC2 cotransporter function in human idiopathic generalized epilepsy. *EMBO Rep* **15:** 766–774.

Kahle KT, Khanna AR, Alper SL, Adragna NC, Lauf PK, Sun D, Delpire E. 2015. K-Cl cotransporters, cell volume homeostasis, and neurological disease. *Trends Mol Med* **21:** 513–523.

Kahle KT, Flores B, Bharucha-Goebel D, Zhang J, Donkervoort S, Hegde M, Hussain G, Duran D, Liang B, Sun D, et al. 2016. Peripheral motor neuropathy is associated with defective kinase regulation of the KCC3 cotransporter. *Sci Signal* **9:** ra77.

Kaplan MR, Plotkin MD, Brown D, Hebert SC, Delpire E. 1996a. Expression of the mouse Na-K-2Cl cotransporter, mBSC2, in the terminal IMCD, the glomerular and extraglomerular mesangium and the glomerular afferent arteriole. *J Clin Invest* **98:** 723–730.

Kaplan MR, Plotkin MD, Lee W-S, Xu Z-C, Lytton J, Hebert SC. 1996b. Apical localization of the Na-K-2Cl cotransporter, rBSC1, on rat thick ascending limbs. *Kidney Int* **49:** 40–47.

Kidokoro M, Nakamoto T, Mukaibo T, Kondo Y, Munemasa T, Imamura A, Masaki C, Hosokawa R. 2014. Na^+-K^+-$2Cl^-$ cotransporter-mediated fluid secretion increases under hypotonic osmolarity in the mouse submandibular salivary gland. *Am J Physiol Renal Physiol* **306:** F1155–F1160.

Laird JM, Garcia-Nicas E, Delpire EJ, Cervero F. 2004. Presynaptic inhibition and spinal pain processing in mice: a possible role of the NKCC1 cation-chloride co-transporter in hyperalgesia. *Neurosci Lett* **361:** 200–203.

Lauf PK, Bauer J, Adragna NC, Fujise H, Zade-Oppen AMM, Ryu K, Delpire E. 1992. Erythrocyte K-Cl cotransport: properties and regulation. *Am J Physiol* **263:** C917–C932.

Law R, Dixon-Salazar T, Jerber J, Cai N, Abbasi AA, Zaki MS, Mittal K, Gabriel SB, Rafiq MA, Khan V, et al. 2014. Biallelic truncating mutations in *FMN2*, encoding the actin-regulatory protein Formin 2, cause nonsyndromic autosomal-recessive intellectual disability. *Am J Hum Genet* **95:** 721–728.

Markadieu N, Delpire E. 2014. Physiology and pathophysiology of SLC12A1/2 transporters. *Pfluegers Arch* **466:** 91–105.

Mathieu V, Chantôme A, Lefranc F, Cimmino A, Miklos W, Paulitschke V, Mohr T, Maddau L, Kornienko A, Berger W, et al. 2015. Sphaeropsidin A shows promising activity against drug-resistant cancer cells by targeting regulatory volume increase. *Cell Mol Life Sci* **72:** 3731–3746.

McKenna A, Hanna M, Banks E, Sivachenko A, Cibulskis K, Kernytsky A, Garimella K, Altshuler D, Gabriel S, Daly M, et al. 2010. The Genome Analysis Toolkit: a MapReduce framework for analyzing next-generation DNA sequencing data. *Genone Res* **20:** 1297–1303.

Moore-Hoon ML, Turner RJ. 2000. The structural unit of the secretory Na^+-K^+-$2Cl^-$ cotransporter (NKCC1) is a homodimer. *Biochemistry* **39:** 3718–3724.

Nezu A, Parvin MN, Turner RJ. 2009. A conserved hydrophobic tetrad near the C terminus of the secretory Na^+-K^+-$2Cl^-$ cotransporter (NKCC1) is required for its correct intracellular processing. *J Biol Chem* **284:** 6869–6876.

O'Mahony F, Toumi F, Mroz MS, Ferguson G, Keely SJ. 2008. Induction of $Na^+/K^+/2Cl^-$ cotransporter expression mediates chronic potentiation of intestinal epithelial Cl^- secretion by EGF. *Am J Physiol Cell Physiol* **294:** C1362–C1370.

Pace AJ, Lee E, Athirakul K, Coffman TM, O'Brien DA, Koller BH. 2000. Failure of spermatogenesis in mouse lines deficient in the Na^+-K^+-$2Cl^-$ cotransporter. *J Clin Invest* **105:** 441–450.

Payne JA, Xu J-C, Haas M, Lytle CY, Ward D, Forbush BI. 1995. Primary structure, functional expression, and chromosome localization of the bumetanide sensitive Na-K-Cl cotransporter in human colon. *J Biol Chem* **270:** 17977–17985.

Pemberton PJ, Valkanas EW, Bone P, Markello CJ, Flynn EJ, Links AE, Boerkoel CF, Adams DR, Gahl WA, Markello TC. 2014. Diploid alignment of whole human genome data. In *Annual society of human genetics*. San Diego, CA.

Plotkin MD, Kaplan MR, Peterson LN, Gullans SR, Hebert SC, Delpire E. 1997. Expression of the Na^+-K^+-$2Cl^-$ cotransporter BSC2 in the nervous system. *Am J Physiol Cell Physiol* **272:** C173–C183.

Randall J, Thorne T, Delpire E. 1997. Partial cloning and characterization of *Slc12a2*: the gene encoding the secretory Na^+-K^+-$2Cl^-$ cotransporter. *Am J Physiol (Cell Physiol.)* **273:** C1267–C1277.

Russell JM. 2000. Sodium-potassium-chloride cotransport. *Physiol Rev* **80:** 211–276.

Schultheis PJ, Lorenz JN, Meneton P, Nieman ML, Riddle TM, Flagella M, Duffy JJ, Doetschman T, Miller ML, Shull GE. 1998. Phenotype resembling Gitelman's syndrome in mice lacking the apical Na^+-Cl^- cotransporter of the distal convoluted tubule. *J Biol Chem* **273:** 29150–29155.

Simard CF, Brunet GM, Daigle ND, Montminy V, Caron L, Isenring P. 2004. Self-interacting domains in the C terminus of a cation-Cl^- cotransporter described for the first time. *J Biol Chem* **279:** 40769–40777.

Simon DB, Karet FE, Hamdan JM, Di Pietro A, Sanjad SA, Lifton RP. 1996a. Bartter's syndrome, hypokalaemic alkalosis with hypercalciuria, is caused by mutations in the Na-K-2Cl cotransporter *NKCC2*. *Nat Genet* **13:** 183–188.

Simon DB, Nelson-Williams C, Johnson Bia M, Ellison D, Karet FE, Morey Molina A, Vaara I, Iwata F, Cushner HM, Koolen M, et al. 1996b. Gitelman's variant of Bartter's syndrome, inherited hypokalaemic alkalosis, is caused by mutations in the thiazide-sensitive Na-Cl cotransporter. *Nat Genet* **12:** 24–30.

Somasekharan S, Tanis J, Forbush B. 2012. Loop diuretic and ion-binding residues revealed by scanning mutagenesis of transmembrane helix 3 (TM3) of Na-K-Cl cotransporter (NKCC1). *J Biol Chem* **287:** 17308–17317.

Stödberg T, McTague A, Ruiz AJ, Hirata H, Zhen J, Long P, Farabella I, Meyer E, Kawahara A, Vassallo G, et al. 2015. Mutations in SLC12A5 in epilepsy of infancy with migrating focal seizures. *Nat Commun* **6:** 8038.

Sung K-W, Kirby M, McDonald MP, Lovinger DM, Delpire E. 2000. Abnormal $GABA_A$-receptor mediated currents in dorsal root ganglion neurons isolated from Na-K-2Cl cotransporter null mice. *J Neurosci* **20:** 7531–7538.

Takahashi N, Chernavvsky DR, Gomez RA, Igarashi P, Gitelman HJ, Smithies O. 2000. Uncompensated polyuria in a mouse model of Bartter's syndrome. *Proc Natl Acad Sci* **97:** 5434–5439.

The 1000 Genomes Project Consortium. 2010. A map of human genome variation from population-scale sequencing. *Nature* **467:** 1061–1073.

Uyanik G, Elcioglu N, Penzien J, Gross C, Yilmaz Y, Olmez A, Demir E, Wahl D, Scheglmann K, Winner B, et al. 2006. Novel truncating and missense mutations of the *KCC3* gene associated with Andermann syndrome. *Neurology* **66:** 1044–1048.

Van der Auwera GA, Carneiro MO, Hartl C, Poplin R, Del Angel G, Levy-Moonshine A, Jordan T, Shakir K, Roazen D, Thibault J, et al. 2013. From FastQ data to high confidence variant calls: the Genome Analysis Toolkit best practices pipeline. *Curr Protoc Bioinformatics* **43:** 11.10.11–11.10.33.

Wei F, Wei MX, Murakami M. 2015. Mechanism involved in Danshen-induced fluid secretion in salivary glands. *World J Gastroenterol* **21:** 1444–1456.

Willems M, Geneviève D, Borck G, Baumann C, Baujat G, Bieth E, Edery P, Farra C, Gerard M, Héron D, et al. 2010. Molecular analysis of pericentrin gene (*PCNT*) in a series of 24 Seckel/microcephalic osteodysplastic primordial dwarfism type II (MOPD II) families. *J Med Genet* **47:** 797–802.

Woo N-S, Lu J, England R, McClellan R, Dufour S, Mount DB, Deutch AY, Lovinger DM, Delpire E. 2002. Hyperexcitability and epilepsy associated with disruption of the mouse neuronal-specific K-Cl cotransporter gene. *Hippocampus* **12:** 258–268.

Wouters M, De Laet A, Ver Donck L, Delpire E, van Bogaert PP, Timmermans JP, de Kerchove d'Exaerde A, Smans K, Vanderwinden JM. 2006. Subtractive hybridization unravels a role for the ion co-transporter NKCC1 in the murine intestinal pacemaker. *Am J Physiol Gastrointest Liver Physiol* **290:** G1219–G1227.

Wu Q, Delpire E, Hebert SC, Strange K. 1998. Functional demonstration of Na-K-2Cl cotransporter activity in isolated, polarized choroid plexus cells. *Am J Physiol Cell Physiol* **275:** C1565–C1572.